ChemPubSoc Europe

DOI: 10.1002/cssc.201402813

CHEMSUSCHEM Full Papers

Bimolecular Crystals with an Intercalated Structure Improve Poly(*p*-phenylenevinylene)-Based Organic Photovoltaic Cells

Kyung-Geun Lim,[a] Jun-Mo Park,[b] Hannah Mangold,[c] Frédéric Laquai,[c] Tae-Lim Choi,*[b] and Tae-Woo Lee*[a]

The exciton dissociation, recombination, and charge transport of bulk heterojunction organic photovoltaic cells (OPVs) is influenced strongly by the nanomorphology of the blend, such as the grain size and the molecular packing. Although it is well known that polymers based on amorphous poly(*p*-phenylenevinylene) (PPV) have a fundamental limit to their efficiency because of low carrier mobility, which leads to increased recombination and unbalanced charge extraction, herein, we demonstrate that the issue can be overcome by forming bimolecular crystals of an amorphous PPV-based polymer:phenyl-C_{61}-butyric acid methyl ester (PCBM) intercalated structure. We used amorphous poly(2,5-dioctyloxy-*p*-phenylene vinylene-*alt*-2′,5′-thienylene vinylene) (PPVTV), which has a simple chemical structure. A reasonably high power conversion efficiency (~3.5%) was obtained, although the material has an intrinsically amorphous structure and a relatively large band gap (2.0 eV). We demonstrate a correlation between a well-ordered bimolecular crystal of PPVTV:PCBM and an improved hole mobility of a PPVTV:PCBM film compared to a pristine PPVTV film by using 2D grazing incidence XRD and space-charge-limited current measurements. Furthermore, we show that the bimolecular crystal structure in high-performance OPVs is related to an optimum molecular packing, which is influenced by the PPVTV:PCBM blending ratio, side-chain length, and molecular weight of the PPVTV polymer. Improved charge transport in PPVTV:PCBM bimolecular crystals leads to a fast sweep out of charges and thus suppression of nongeminate recombination under the operating conditions.

Introduction

Organic photovoltaic (OPV) devices have received great attention because they exhibit several advantages, such as flexibility, solution processability, and low weight.[1] Specifically, bulk heterojunction (BHJ) solar cells that use amorphous poly(*p*-phenylenevinylene) (PPV) as a donor and phenyl-C_{61}-butyric acid methyl ester (PCBM) as an acceptor material enabled a dramatic improvement in power conversion efficiency (PCE) through nano-sized phase separation and ultrafast electron transfer from the polymer to PCBM.[2] Further improvement was achieved by using regioregular semicrystalline poly(3-hexylthiophene) (rr-P3HT) as a donor polymer, which exhibits a smaller band gap and higher hole mobility than PPV.[3] Since then, the PCE has been improved continuously, and recently 5–8% was reached through the development of various low-band-gap polymers as donor materials, for example, PCPDTBT (poly[2,6-(4,4-bis-(2-ethylhexyl)-4*H*-cyclopenta[2,1-b;3,4-b′]-dithiophene)-*alt*-4,7-(2,1,3-benzothiadiazole)]),[4] PCDTBT(poly[*N*-9′′-heptadecanyl-2,7-carbazole-alt-5,5-(4′,7′-di-2-thienyl-2′,1′,3′-benzothiadiazole),[5] PBDTTT-CF (poly[4,8-bis-substituted-benzo [1,2-b:4,5-b′]dithiophene-2,6-diyl-alt-4-substituted-thieno[3,4-b]thiophene-2,6-diyl]).[6] However, there has been little improvement in terms of the cost of fabrication because the synthesis of these new materials can be challenging, which diminishes the benefit of low-cost processing as one of the key advantages of OPV technology.

PPVs are easy to prepare and commercially available and these amorphous conjugated polymers were studied extensively at the beginning of OPV research.[1] However, they have received little attention since the introduction of rr-P3HT, which exhibits a good performance as a donor polymer. Furthermore, the low hole mobility of PPVs causes not only poor charge carrier extraction that leads to enhanced recombination but also to unbalanced charge transport (hole mobility of 5×10^{-7} $cm^2V^{-1}s^{-1}$ for PPV [poly(paraphenylene vinylene)][7] and electron mobility of 2×10^{-3} $cm^2V^{-1}s^{-1}$ for PCBM[8]), which in turn leads to a low fill factor (FF). Thus, a further improvement of the hole mobility is necessary to achieve higher PCEs in BHJ solar cells. Recently, Tajima and co-workers reported the preparation of regioregular and crystalline PPV with an improved hole mobility,[9] and as a result they obtained polymer BHJ

[a] K.-G. Lim, Prof. T.-W. Lee
Department of Materials Science and Engineering
Pohang University of Science and Technology (POSTECH)
San 31 Hyoja-dong, Nam-gu, Pohang, Gyungbuk 790-784 (South Korea)
E-mail: twlee@postech.ac.kr

[b] J.-M. Park, Prof. T.-L. Choi
Department of Chemistry
College of Natural Sciences
Seoul National University
Seoul 151-747 (South Korea)
E-mail: tlc@snu.ac.kr

[c] Dr. H. Mangold, Dr. F. Laquai
Max Planck Research Group for Organic Optoelectronics
Max Planck Institute for Polymer Research
Ackermannweg 10, 55128 Mainz (Germany)

solar cells with a PCE of 3.1 %.[10] To increase the hole mobility, one can improve the crystallinity of the donor polymers, however, this also increases the sensitivity with respect to its thermal history, which in turn can cause large-scale phase separation in the film during the thermal annealing step.[11] In this regard, despite their low mobility, amorphous conjugated polymers are less sensitive to their thermal history and also provide a uniform bulk for charge transport.[12] Recently, we developed an amorphous PPV-type copolymer by the Horner–Emmons reaction.[13] These polymers have a simple structure and show a relatively high field-effect hole mobility compared to other amorphous conjugated polymers.[13] Notably, this polymerization procedure involves no transition metals, whereas many other polymers used in OPV devices contain metal residues such as Pd, which can potentially be a problem in manufacturing processes in industry.

Herein, we report the application of poly(2,5-dioctyloxy-*p*-phenylene vinylene-*alt*-2′,5′-thienylene vinylene) (PPVTV) in OPVs and its unusual packing motif in thin films. As a result, we demonstrate that the polymer, which is easy to prepare because of its simple chemical structure, yields reasonably high performance PPV-based OPVs with a PCE of 3.5 % because of its well-ordered bimolecular crystal formation in PPVTV:PCBM thin films and improved hole mobility, although PPVTV has an intrinsically amorphous structure and a large band gap (~2.0 eV). 2D grazing incidence X-ray diffraction (GIXD) and space-charge-limited current (SCLC) measurements revealed that a well-ordered bimolecular crystal of PPVTV:PCBM improved the hole mobility of a PPVTV:PCBM film compared to a pristine PPVTV film. We also find that an optimum molecular packing to form well-ordered bimolecular crystals is influenced by the PPVTV:PCBM blending ratio, side-chain length, and molecular weight of the PPVTV polymer. In addition, the improved charge transport in PPVTV:PCBM bimolecular crystals leads to the fast extraction of spatially separated charges and thus the suppression of nongeminate recombination of free carriers.

Results and Discussion

PPVTV exclusively as the *trans* olefin isomer was prepared by following a typical Horner–Emmons reaction procedure (Scheme 1).[13] The PPVTV polymer has a high number-averaged molecular weight (M_n) of 63 kDa and a polydispersity index (PDI) of 2.75 as measured by gel permeation chromatography (GPC). To determine the electrochemical properties of the prepared polymer, the HOMO, LUMO, and band gap were measured by cyclic voltammetry and UV/Vis absorption spectroscopy (Table 1). The band gap was 2.0 eV, and the HOMO was determined to be 5.1 eV, which is slightly higher than that of P3HT (5.0 eV).[11]

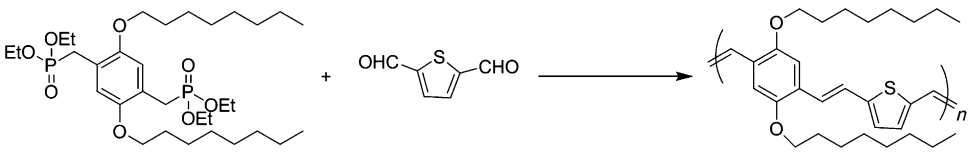

Scheme 1. Synthesis of PPVTV.

Table 1. Molecular weights and energy levels of PPVTV.

M_n[a]	M_w[a]	PDI[a]	E_g^{op}[b] [eV]	HOMO[c] [eV]	LUMO[d] [eV]
63k	173k	2.75	2.0	−5.1	−3.1

[a] Molecular weights and polydispersity index were determined by THF GPC relative to polystyrene standards. [b] Estimated from the onset of UV/Vis absorption data of the thin film. [c] Calculated from the oxidation onset potentials under the assumption that the absolute energy level of ferrocene/ferrocenium (Fc/Fc^+) was −4.8 eV under a vacuum (cf. P3HT = −5.02 eV). [d] HOMO$-E_g^{op}$.

2D GIXD patterns of thin films of PPVTV, PCBM, and a PPVTV/PCBM (1:4 w/w) blend measured at a grazing incidence angle of $\alpha_i = 0.4^\circ$ are shown in Figure 1. In the GIXD image of the PPVTV film (Figure 1a), no order was found except the broad and diffuse peak in the out-of-plane direction, which corresponds to a stacking distance of 1.62 $Å^{-1}$. The neat PCBM film showed a broad halo at 1.41 $Å^{-1}$ as a result of scattering by fullerene (Figure 1b), which indicates that the PCBM is amorphous, that is, that no preferential ordering of the PCBM domains was present.[14,15] However, several scattering spots with regular spacing were observed in the GIXD image of the PPVTV:PCBM 1:4 film (Figure 1c). The scattering spots satisfy the Bragg conditions for a hexagonal reciprocal lattice in the PPVTV:PCBM plane. The GIXD pattern contains reflection spots in the direction of 60° (1 0), 30° (1 1), and out-of-plane (0 1). These scattering spots of [1 0], [1 1], and [0 1] were not found in neat PPVTV or neat PCBM films because there is no periodic plane or ordering that reflects the incident X-rays (Figure 1a and b). The GIXD patterns of PPVTV (M_n of 63 kDa):PCBM 1:4 blend films also contain the broad halo identical to that seen in Figure 1b, which corresponds to an amorphous PCBM phase in blend films. This indicates that a bimolecular crystal with a hexagonal lattice and an amorphous PCBM phase are formed simultaneously in the PPVTV:PCBM 1:4 blend film.

Based on the GIXD patterns, we propose that PPVTV and PCBM pack according to a hexagonal ABAB plane sequence (Figure 2). From the hexagonal array of diffraction spots indexed as shown in Figure 1c, a *d* spacing of 7.46 and 4.60 Å was deduced that corresponds to reciprocal lattice vectors of [0 1] and [1 1], respectively. The hcp (hexagonal close pacing) *c*/*a* ratio of PPVTV:PCBM is 1.622 ($a = 9.20$, $c = 14.92$ Å), which is close to the ideal hcp sphere packing *c*/*a* ratio of $\sqrt{8/3} = 1.633$.

Unlike P3HT and BEH-BMB-PPV (poly[2,5-bis(2-ethylhexyloxy)-co-2,5-bis(methylbutyloxy)-1,4-phenylene vinylene]),[15] PPVTV has sufficient free volume to accommodate PCBM mole-

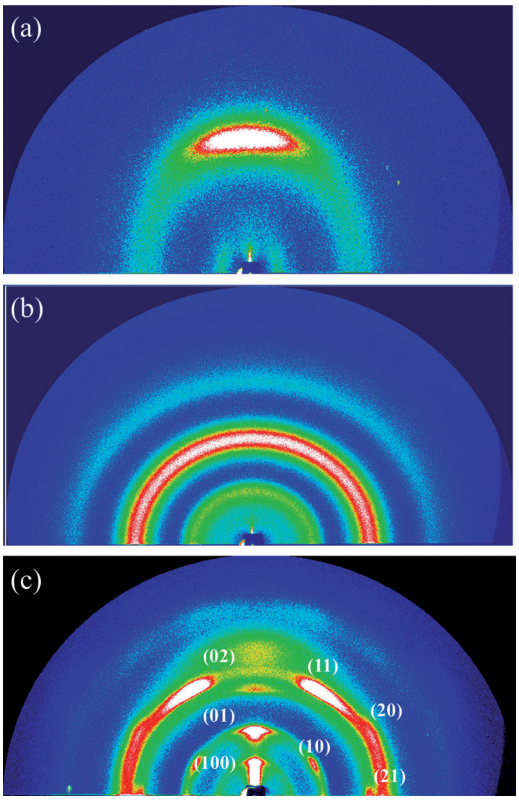

Figure 1. Grazing incidence wide-angle X-ray scattering patterns of spin-cast a) PPVTV, b) PCBM, and c) PPVTV:PCBM blend thin film.

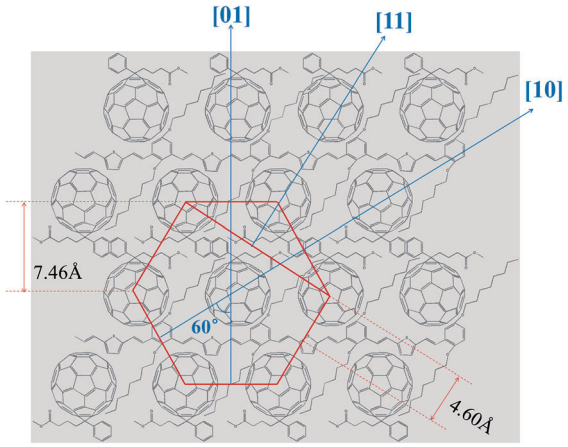

Figure 2. Schematic representation of the 2D hcp structure formed in a PPVTV:PCBM blend thin film.

cules between the alkyl side chains (Figure 2). The bimolecular crystals of semiconducting molecules can give rise to certain optoelectronic properties such as strong charge-transfer (CT) states.[15] In short, the GIXD results indicate that PPVTV:PCBM films consist of an hcp structure of polymer-PCBM intercalating bimolecular crystals.

We demonstrate hole transport in PPVTV (M_n of 63 kDa):PCBM films by SCLC measurements to evaluate the carrier mobility under steady-state conditions in an organic layer.[16] The hole transport in the intercalated structure was evaluated by comparing the hole mobility of PPVTV:PCBM blends with that of pristine PPVTV films. We have estimated the hole mobility of hole-only devices with an Ohmic hole contact by the introduction of a high-work-function poly(3,4-ethylenedioxythiophene) (PEDOT):polystyrene sulfonate (PSS) layer (5.48 eV). The work function of PEDOT:PSS was controlled by mixing a PEDOT:PSS Baytron PH solution with the perfluorinated ionomer (PFI)[17] because the key requirement of SCLC mobility measurements is an Ohmic contact between the organic layer and the anode. In other words, an appropriate hole-injecting buffer layer that has Ohmic contacts for the hole injection makes it feasible to utilize SCLC measurements for mobility determination.

The hole mobility of PPVTV:PCBM films and neat PPVTV films was estimated as 1.41×10^{-4} and 1.02×10^{-4} $cm^2V^{-1}s^{-1}$, respectively, at an electric field of 0.36 $MV\,cm^{-1}$ (Figure 3). The

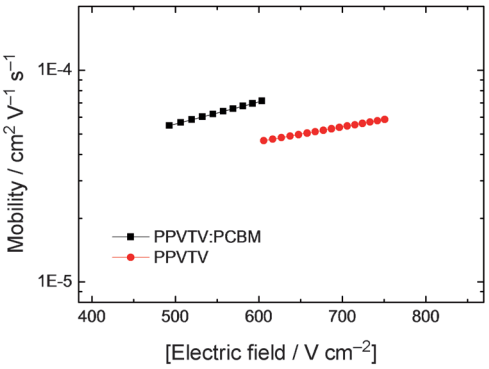

Figure 3. Hole mobility of PPVTV and PPVTV:PCBM film estimated by SCLC measurements.

hole mobility and current density of PPVTV:PCBM blend films are higher than the hole mobility of neat PPVTV. Importantly, the hole mobility of the polymer increased even though it was mixed with n-type PCBM, which may limit the hole transport pathways in the blend. The increased hole mobility appears to be related to the intercalating hexagonal packing, because the intercalation of PCBM between PPVTV side chains may lead to the uncoiling and stretching-out of the polymer chains.

For the complete intercalation to occur, a high polymer:PCBM ratio such as a blend ratio of 1:3 to 1:4 is necessary because at lower ratios, the intercalation is incomplete or less effective.[15] To show that intercalation and a bimolecular crystal structure occur and that in turn the device characteristics change drastically, we studied the device properties as a function of the PPVTV (M_n of 63 kDa):PCBM ratio. If the device was fabricated with a PPVTV:PCBM blend with a 1:2 ratio, a limited charge transport and much lower PCE (0.6%) was obtained compared to that with a 1:4 blend (3.5%; Figure 4a). The device with a 1:2 blend showed a higher series resistance of 376 $\Omega\,cm^2$ and lower FF of 18.5% compared to the blend with a 1:4 ratio (7 $\Omega\,cm^2$ and 61.4%, respectively). This could be ad-

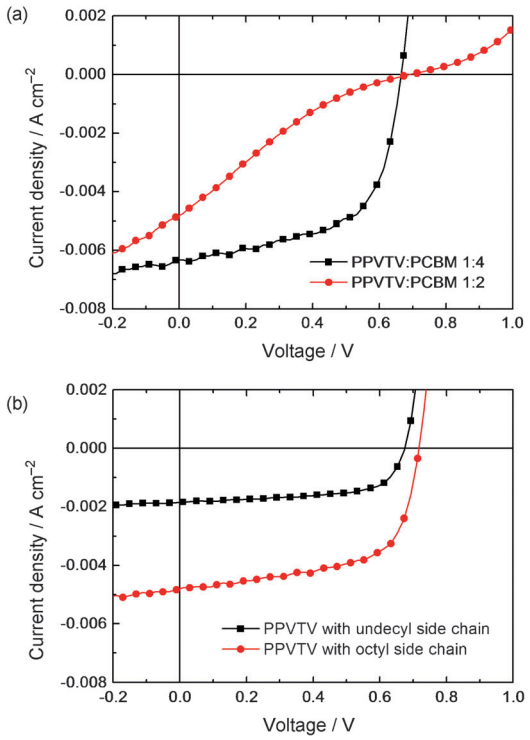

Figure 4. *J–V* characteristics that depend on (a) PPVTV:PCBM ratio and (b) side-chain length of PPVTV.

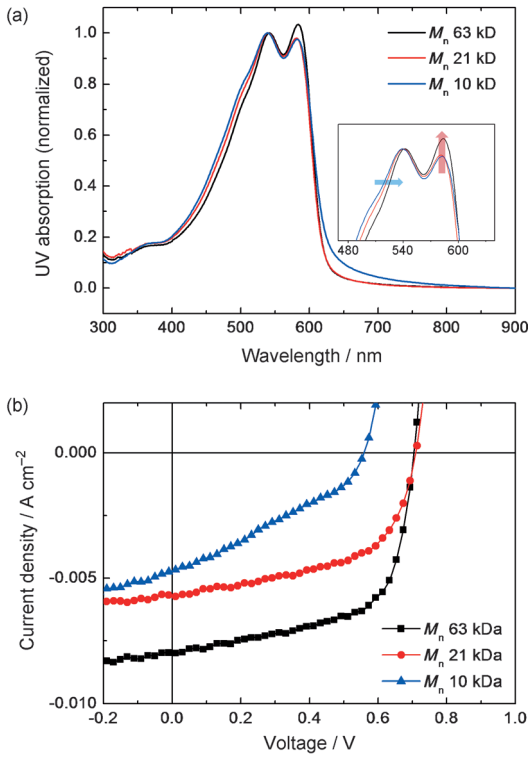

Figure 5. Effect of the molecular weight of PPVTV on (a) the UV absorption spectrum and (b) *J–V* characteristics.

ditional evidence for PPVTV:PCBM intercalation, which leads to a bimolecular crystal.

The side-chain length of PPVTV (M_n of 63 kDa) also impacts significantly on the short-circuit current J_{sc} of the corresponding BHJ solar cell (Figure 4b). The longer undecyl side chain provides weaker intermolecular interaction in the polymer:PCBM blends than the parent polymer that has an octyl side chain, which results in a reduced J_{sc} (4.8 mA cm^{-2} for the octyl chain and 2.2 mA cm^{-2} for the undecyl chain).

The UV/Vis absorption spectrum of the PPVTV film is shown in Figure 5a. Notably, the polymer shows a strong shoulder at around $\lambda = 600$ nm, which indicates stacking and is also in good agreement with the GIXD analysis (Figure 1a). In addition, this shoulder increases with the increasing molecular weight of the polymer, which indicates enhanced stacking. This is also reflected in the higher field-effect hole mobility of a higher molecular weight PPVTV (5.6×10^{-2} cm^{2}V^{-1}s^{-1} for a polymer with $M_n = 63$ kDa vs. 1.4×10^{-2} cm^{2}V^{-1}s^{-1} for that with $M_n = 16$ kDa).[13] Notably, similar results were also reported by Müllen et al.[18]

In the OPV figures of merit, a clear correlation between the molecular weight of the polymer and the device performance was observed. The performance of BHJ solar cells based on PPVTV with three different molecular weights ($M_n = 10$, 21, and 63 kg mol^{-1}) are shown in Figure 5b. With the increasing molecular weight, an increase of J_{sc} is observed from 4.7 mA cm^{-2} for $M_n = 10$ kg mol^{-1} to 8 mA cm^{-2} for $M_n = 63$ kg mol^{-1}. In addition the FF increases significantly from 31.9% to 61.4%. As a result, these changes lead to an increase in the PCE from 0.8% and 2.2% to 3.5%. We believe that the increase in hole mobility is responsible for the enhanced OPV performance.[19]

To gain an insight into the charge generation and loss processes in the most efficient PPVTV (M_n of 63 kDa):PCBM 1:4 sample, transient absorption pump-probe (TA) spectroscopy was performed. The spectra of the blend at time delays between 1 ps and 1 ns after excitation at 532 nm are presented in Figure 6a. A pronounced ground state bleach (GSB) is observed at around 600 nm, which coincides with the absorption of the blend. The GSB exhibits a redshift and broadening in the first nanosecond because of the spectral relaxation of charges in the density of states as reported previously for other OPV blends.[20] A small signal caused by stimulated emission is observed at around 700 nm, however, it is completely quenched after 10 ps, which indicates fast exciton quenching and CT at the interface with PCBM after PPVTV excitation. A broad photoinduced absorption (PIA) is observed in the wavelength range from 750–950 nm. If we take a closer look at the kinetics (Figure 6b), different processes can be distinguished. After a fast initial exciton quenching and CT, an increase of the charge-induced absorption signal is observed for the lower excitation intensities during the first 50 ps. We ascribe this rise to delayed charge formation caused by slow exciton diffusion in PCBM-rich domains, which causes delayed charge separation at the interface with the polymer.[20] As PCBM accounts for 80 wt% of the blend, this effect is substantial. The increase in signal is more distinct for lower excitation intensities as exciton annihilation processes that counteract and suppress the signal increase at higher intensities. After approximately 200 ps, the

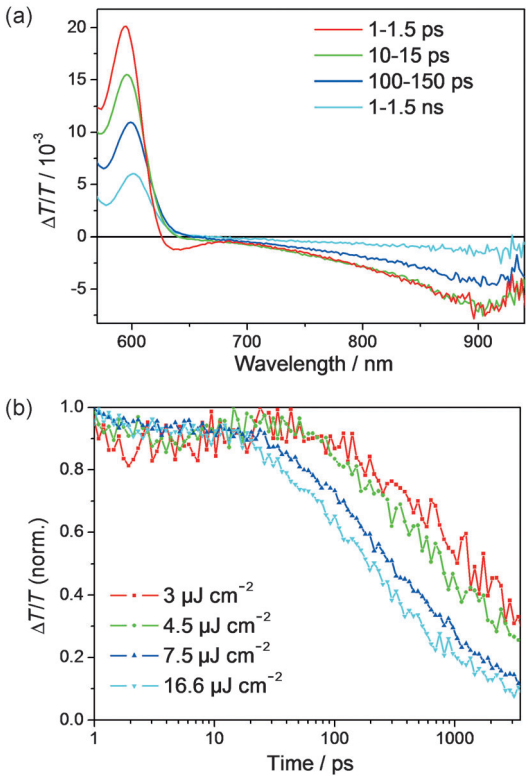

Figure 6. (a) The ps–ns transient absorption spectra of the PPVTV:PCBM (1:4) blend at time delays specified in the spectra after excitation at 530 nm. (b) Kinetics in the wavelength region of the photoinduced absorption (800–900 nm).

kinetics exhibit a monoexponential decay for all measured intensities. A global fit of the data at different intensities to a single-exponential decay function reveals a mean lifetime of 990 ps. From 200 ps to 3 ns, geminate recombination of bound charge pairs or CT states is observed.

As a considerable proportion of the signal remained after 3 ns, we investigated the dynamics on timescales up to microseconds, in which the recombination of free charge carriers is usually observed. Specifically, we investigated the dynamics in the PIA region between $\lambda = 700$ and 900 nm at different excitation intensities (Figure 7). The solid black lines represent fits to a model of concomitant recombination of bound and free charges that we have developed and applied to fit the recombination dynamics in P3HT:PCBM blends[22] as well as in PCDTBT and PCPDTBT blends.[20,21] The model assumes that after 1 ns, that is, at the beginning of the ns–μs TA experiment, the exciton dissociation is already finished and the charge carrier population is split into two pools: bound CT states and free (spatially separated or mobile) charge carriers. The former recombine exclusively by geminate recombination to the ground state (GS), whereas the spatially separated (free) charge carriers (SCC) recombine nongeminately. Interconversion between the two pools is excluded deliberately in our model, as the CT states observed on this timescale are relaxed into bound states. We further assume that CT states and free charge carriers have equal absorption cross-sections in the wavelength region used for our analysis. This assumption appears to be valid as the spectral shape does not change during the entire TA measurement. The recombination dynamics are then fitted globally, and the following values can be extracted from the fit: (i) the branching ratio of the geminate versus nongeminate recombination fraction f (which is equal to the branching ratio between the CT states and free charges at the beginning of the experiment), specifically the fraction f of free charge carriers that undergo nongeminate recombination, (ii) the geminate (exponential) recombination rate constant $k_{CT \rightarrow GS}$, (iii) the nongeminate recombination coefficient γ, and (iv) the order of the nongeminate recombination process $\lambda+1$. The obtained values are summarized in Table 2. Roughly half of the excitons form free charge carriers ($f = 0.46$), whereas the other half forms tightly bound CT states that decay at a rate of 7.5×10^8 s^{-1}, which corresponds to a lifetime of 1.3 ns and compares well with the results obtained from the short-delay (ps–ns) TA measurements given that the temporal resolution of our ns–μs TA experiment is limited to approximately 1 ns. Notably, our TA experiments are performed in the absence of an electric field, that is, under open-circuit conditions. Hence, a fraction of 46% of free charge formation is the lower limit for the yield of free charges in these blends, which could

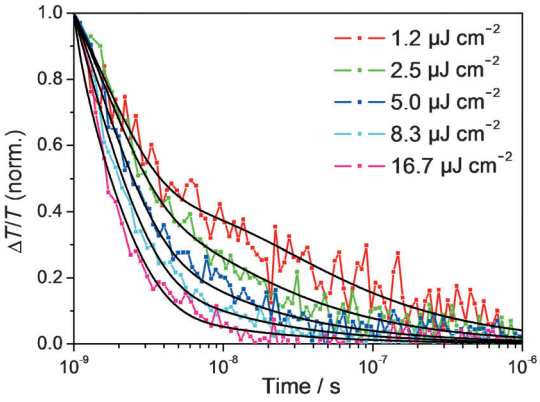

Figure 7. Intensity dependence of the long-delay (ns–μs) decay dynamics of the photoinduced absorption in the PPVTV:PCBM (1:4) blend after excitation at 532 nm. The colored dotted lines correspond to the experimental data, and the black lines are fits obtained from a photophysical model as described in the text.

Table 2. Fitting parameters with standard deviations extracted from a global fit of the photoinduced absorption kinetics (700–900 nm) in the long-delay measurement according to the model described above. For the quality of the fit see Figure 7. The parameters were shared for all excitation intensities. f is the fraction of nongeminate recombination, γ is the nongeminate decay constant, $\lambda+1$ is the order of the nongeminate recombination, k is the geminate recombination rate, and γ_{eff} is the effective ($\lambda+1 = 2$) bimolecular recombination constant at a charge density of 5×10^{15} cm^{-3}.

f	γ [(cm^3)$^\lambda$ s^{-1}]	$\lambda+1$	k [s^{-1}]	γ_{eff} [cm^{-3} s^{-1}]
0.46 ± 0.01	$(2.3 \pm 1.8) \times 10^{-18}$	2.51 ± 0.02	$(7.5 \pm 0.3) \times 10^8$	$(3 \pm 2) \times 10^{-10}$

be larger at higher device bias. In the operating bias range of the solar cell, the photocurrent shows a bias dependence (indicated by the slope of the *J*–*V* curves), which indicates a field-activated charge separation process. However, nongeminate recombination of free charge carriers could also be an additional loss channel, as the effective Langevin recombination coefficient calculated for bimolecular ($\lambda+1=2$) recombination at a charge carrier density of $5\times10^{15}\,cm^{-3}$ is of the order of $10^{-10}\,cm^3\,s^{-1}$, which is distinctly larger than that observed for annealed P3HT:PCBM films, for example, in which γ_{eff} (the effective bimolecular recombination coefficient) is of the order of $10^{-13}\,cm^3\,s^{-1}$.[22] Hence, in the investigated PPVTV:PCBM films, nongeminate recombination of free charges is fast and could compete with charge carrier extraction. However, the FF of the devices is still high (61%), most likely because of the high hole and electron mobilities observed for PPVTV:PCBM bimolecular crystals, which leads to a fast sweeping out of charges and thus suppression of nongeminate recombination under the operating conditions. This can explain the comparably high device performance even though nongeminate recombination is fast and a significant fraction of bound CT states is formed upon exciton dissociation.

Conclusions

We have shown that poly(2,5-dioctyloxy-*p*-phenylene vinylene-*alt*-2′,5′-thienylene vinylene) (PPVTV), based on poly(*p*-phenylenevinylene) (PPV), produced a reasonably high power conversion efficiency (PCE) up to 3.5% in organic photovoltaic devices, which is surprising because the polymer is intrinsically amorphous. We found that a thin film of a PPVTV:phenyl-C_{61}-butyric acid methyl ester (PCBM) blend shows well-ordered bimolecular crystals of hexagonal close packing as determined by 2D grazing incidence X-ray diffraction, which resulted in a great improvement of the PCE. As a result of the intercalation of PCBM between the PPVTV side chains, the blend shows improved hole mobility compared to pristine PPVTV as determined by space-charge-limited current measurements. The OPV performance is influenced strongly by the PPVTV:PCBM blending ratio, length of the side chains, and molecular weight of PPVTV. By transient optical spectroscopy, we determined that exciton quenching is rather fast in these PPVTV:PCBM 1:4 blends, which ensures efficient charge transfer. However, upon exciton dissociation only half of the initial states create free charges under open-circuit conditions, and the other half forms bound charge-transfer states, which recombine geminately with an inverse rate of approximately 1 ns. Despite the relatively high fraction of charge-transfer-state formation the solar cells are reasonably efficient, as those charges, which are separated spatially, are extracted quickly from the photoactive layer to thereby reduce nongeminate recombination of free charges and lead to high fill factors. In addition, further research on device stability is needed because the intermolecular structure in the bimolecular crystal is expected to be thermodynamically stable to overcome a shortage of vinylene materials in device stability.[24,25]

Experimental Section

Synthesis

Anhydrous solvents, 2,5-thiophenedicarboxaldehyde, and 1 M potassium *tert*-butoxide in THF were purchased from Aldrich. 1,4-Bis-(diethylphosphonate)-2,5-dioctyloxybenzene was prepared by a known method.[23] ^{1}H NMR and UV/Vis spectra were measured by using a Varian/Oxford As-500 (500 MHz) spectrometer, Jasco Inc and UV/Vis-Spectrometer V-550, respectively. GPC was performed by using a Waters system and a Shodex GPC LF-804 column eluted with THF. The cyclic voltammetric waves were measured by using a Zahner IM6eX electrochemical workstation with a 0.1 M acetonitrile solution that contained tetrabutylammonium hexafluorophosphate (Bu_4NPF_6) as the electrolyte at a constant scan rate of $50\,mV\,s^{-1}$. Indium tin oxide (ITO), a Pt wire, and silver/silver chloride (Ag in 0.1 M KCl) were used as the working, counter, and reference electrodes, respectively.

PPVTV: To a flask charged with two monomers in THF solution, 1 M *t*BuOK solution in THF was added dropwise. The reaction was heated to reflux for 12 h under an Ar atmosphere. The polymerization was quenched by the addition of aqueous ammonium chloride. After aqueous work-up, the polymer solution was precipitated into excess methanol, followed by Soxhlet extraction with methanol, acetone, and hexane for 12 h each. The remaining polymer in the thimble was dried overnight in vaccuo. Yield: 80%; $M_n=63\,000\,g\,mol^{-1}$; GPC: PDI = 2.75; ^{1}H NMR (500 MHz, $CDCl_3$): $\delta=7.2$–7.3 (m, 4H), 7.0 (s, 2H), 6.9 (s, 2H), 4.0 (t, 4H), 1.9 (t, 4H), 1.6 (m, 4H), 1.2–1.4 (br, 16H), 0.9 ppm (t, 6H).

Device fabrication

A PEDOT:PSS (CLEVIOS PH) dispersion was diluted in isopropyl alcohol with a 1:1 volume ratio and then spin-coated to give a 35 nm thick hole-extraction layer on top of ITO/glass, followed by baking on a hotplate in air at 200 °C for 10 min. The photoactive layer was composed of a 1:4 mixture of PPVTV and PCBM (from nano-C Inc.) in anhydrous 1,2-dichlorebenzene (DCB; Sigma Aldrich, Inc). PPVTV:PCBM:DCB (6 mg:24 mg:1 mL) solution was heated at 60 °C for 12 h for good homogeneity. After the PEDOT:PSS/ITO substrates were moved to a N_2-filled glovebox, the blend solution was spin-coated on the PEDOT:PSS to give a thickness of 67 nm. The substrates were baked by using a vacuum hotplate at 70 °C for 15 min. The BaF_2 interlayer was thermally evaporated on the blend film at a deposition rate of $0.1\,Å\,s^{-1}$ under high vacuum ($<5\times10^{-7}$ Torr), and the Al cathode was deposited sequentially: first, 20 nm thickness at a rate of $1\,Å\,s^{-1}$ and then 80 nm thickness at a deposition rate of $5\,Å\,s^{-1}$ under high vacuum ($<5\times10^{-7}$ Torr). The photoactive area ($0.06\,cm^2$) was defined by metallic shadow masks. The devices were encapsulated with a glass lid using a UV-curable epoxy resin in a N_2-filled glovebox.

Device characterization

The current density–voltage (*J*–*V*) characteristics were obtained using a computer-controlled Keithley 2400 source measurement unit under simulated solar AM 1.5G illumination at an intensity of $100\,mW\,cm^{-2}$ generated using a Xenon lamp-based solar simulator system (Newport 69907, Class AAA, 450 W).

GIXD characterization

PPVTV:PCBM:DCB (6 mg:24 mg:1 mL) and PPVTV:DCB (20 mg:1 mL) solutions were heated at 60 °C for 12 h for good homogeneity. After coating the PEDOT:PSS on a silicon substrate, each solution was spin-coated on the glass/PEDOT:PSS and heated at 70 °C for 15 min. GIXD measurements were performed at the 4C2 beamline at the Pohang Accelerator Laboratory. Patterns were measured with an X-ray radiation source of $\lambda = 0.154$ nm and imaged by using a 2D charge-coupled detector (CCD: Roper Scientific, Trenton, NJ, USA). Scattering angles were corrected according to the positions of the X-ray beams reflected from the silicon substrate interface with the changing incidence angle α_i, and with respect to a precalibrated silver behenate (TCI, Japan) powder. Aluminum foil pieces were employed as semitransparent beam stops because the intensity of the specular reflection from the substrate is much stronger than the intensity of the GIXD near the critical angle.

TA measurements

TA measurements were performed with a home-built pump-probe setup. To measure in the time range of 1 ps to 4 ns with a resolution of ~100 fs, the output of a commercial titanium:sapphire amplifier (Coherent LIBRA HE, 3.5 mJ, 1 kHz, 100 fs) was split into two beams. Both beams were used to pump an optical parametric amplifier (Coherent OPerA Solo), one to generate a 1300 nm seed pulse for white-light generation with a sapphire window in the visible and the other to generate an excitation pulse at 530 nm. The variable delay of up to 4 ns between pump and probe was introduced by a broadband retroreflector mounted on a mechanical delay stage. Only reflective elements were used to guide the probe beam to the sample to minimize chirp. The excitation pulse was chopped at 500 Hz, and the white-light pulses were dispersed onto a linear photodiode array, the readout of which was 1 kHz. Adjacent diode readings that correspond to the transmission of the sample after an excitation pulse and without an excitation pulse were used to calculate $\Delta T/T$. To measure in the time range of 1 ns to 1 ms with a resolution of 600 ps, the excitation pulse was provided by an actively Q-switched Nd:YVO4 laser (AOT Ltd. MOPA) at 532 nm. The delay between the pump and probe in this case was controlled by an electronic delay generator (Stanford Research Systems DG535). TA measurements were performed at RT under dynamic vacuum at pressures lower than 10^{-5} mbar. Films were prepared analogously to that of the solar cells with the best efficiencies. Polymer and PCBM were mixed in a 1:4 ratio in *ortho*-dichlorobenzene with a total concentration of 30 mg mL^{-1}. The solution was stirred at 70 °C overnight. Films were spin-coated on precleaned and argon-plasma-activated quartz substrates with a spin speed of 2000 rpm. This resulted in layer thicknesses of approximately 65 nm.

Acknowledgements

This work was supported by the National Research Foundation of Korea(NRF) grant funded by the Korea government(MSIP) (NRF-2013R1A2A2A01068753). F.L. thanks the Max Planck Society for funding a Max Planck Research Group. T-L. C is grateful for financial support from the Basic Science Research Program and the Nano-Material Technology Development Program through NRF.

Keywords: absorption · electron transfer · polymers · thin films · x-ray diffraction

[1] a) S. Günes, H. Neugebauer, N. S. Sariciftci, *Chem. Rev.* **2007**, *107*, 1324 – 1338; b) J. You, L. Dou, K. Yoshimura, T. Kato, K. Ohya, T. Moriarty, K. Emery, C.-C. Chen, J. Gao, G. Li, Y. Yang, *Nat. Commun.* **2013**, *4*, 1446; c) K. Cnops, B. P. Rand, D. Cheyns, B. Verreet, M. A. Empl, P. Heremans, *Nat. Commun.* **2014**, *5*, 3406; d) J. H. Park, T.-W. Lee, B.-D. Chin, D. H. Wang, O. O. Park, *Macromol. Rapid Commun.* **2010**, *31*, 2095 – 2108; e) T.-W. Lee, K.-G. Lim, D.-H. Kim, *Electron. Mater. Lett.* **2010**, *6*, 41 – 50; f) S. Ochiai, P. Kumar, K. Santhakumar, P.-K. Shin, *Electron. Mater. Lett.* **2013**, *9*, 399 – 403; g) P.-H. Wang, H.-F. Lee, Y.-C. Huang, Y.-J. Jung, F.-L. Gong, W.-Y. Huang, *Electron. Mater. Lett.* **2014**, *10*, 767 – 773; h) F. C. Krebs, N. Espinosa, M. Hösel, R. R. Søndergaard, M. Jørgensen, *Adv. Mater.* **2014**, *26*, 29 – 39; i) R. R. Søndergaard, M. Hösel, F. C. Kreb, *J. Polym. Sci. Part B* **2013**, *51*, 16 – 34; j) K. G. Lim, M. R. Choi, J. H. Kim, D. H. Kim, G. H. Jung, Y. Park, J. L. Lee, T. W. Lee, *ChemSusChem* **2014**, *7*, 1125 – 1132; k) M. R. Choi, T. H. Han, K. G. Lim, S. H. Woo, D. H. Huh, T. W. Lee, *Angew. Chem. Int. Ed.* **2011**, *50*, 6274; *Angew. Chem.* **2011**, *123*, 6398; l) K. G. Lim, M. R. Choi, H. B. Kim, J. H. Park, T. W. Lee, *J. Mater. Chem.* **2012**, *22*, 25148 – 25153; m) D. H. Kim, K. G. Lim, J. H. Park, T. W. Lee, *ChemSusChem* **2012**, *5*, 2053 – 2057; n) S. Kwon, K. G. Lim, M. Shim, H. C. Moon, J. Park, G. Jeon, J. Shin, K. Cho, T. W. Lee, J. K. Kim, *J. Mater. Chem. A* **2013**, *1*, 11802 – 11808.

[2] S. E. Shaheen, C. J. Brabec, N. S. Sariciftci, *Appl. Phys. Lett.* **2001**, *78*, 841 – 843.

[3] a) F. Padinger, R. S. Rittberger, N. S. Sariciftci, *Adv. Funct. Mater.* **2003**, *13*, 85 – 88; b) P. Schilinsky, C. Waldauf, C. J. Brabec, *Appl. Phys. Lett.* **2002**, *81*, 3885 – 3888; c) J. Kim, S. Kim, H. Lee, K. Lee, W. Ma, X. Gong, A. J. Heeger, *Adv. Mater.* **2006**, *18*, 572 – 576.

[4] S. Park, A. Roy, S. Beaupre, S. Cho, N. Coates, J. Moon, M. L. Daniel Moses, K. Lee, A. J. Heeger, *Nat. Photonics* **2009**, *3*, 297 – 303.

[5] J. Peet, J. Y. Kim, N. E. Coates, W. L. Ma, D. Moses, A. J. Heeger, G. C. Bazan, *Nat. Mater.* **2007**, *6*, 497 – 500.

[6] H. Chen, J. Hou, S. Zhang, Y. Liang, G. Yang, Y. Yang, L. Yu, G. Li, *Nat. Photonics* **2009**, *3*, 649 – 653.

[7] P. W. M. Blom, M. J. M. de Jong, M. G. van Munster, *Phys. Rev. Lett. B* **1997**, *55*, R656 – R659.

[8] V. D. Mihailetchi, J. K. J. van Duren, P. W. M. Blom, J. C. Hummelen, R. A. J. Janssen, J. M. Krroon, M. T. Rispens, W. Verhees, M. M. Wienk, *Adv. Funct. Mater.* **2003**, *13*, 43 – 46.

[9] Y. Suzuki, K. Hashimoto, K. Tajima, *Macromolecules* **2007**, *40*, 6521 – 6528.

[10] K. Tajima, Y. Suzuki, K. Hashimoto, *J. Phys. Chem. C* **2008**, *112*, 8507 – 8510.

[11] a) C. H. Woo, B. C. Thompson, B. J. Kim, M. F. Toney, J. M. J. Frechet, *J. Am. Chem. Soc.* **2008**, *130*, 16324 – 16329; b) K. Sivula, C. K. Luscombe, J. M. J. Frechet, *J. Am. Chem. Soc.* **2006**, *128*, 13988 – 13989.

[12] H. Sirringhaus, *Adv. Mater.* **2005**, *17*, 2411 – 2425.

[13] T.-L. Choi, K. Han, J. Park, D. Kim, J. Park, S. Lee, *Macromolecules* **2010**, *43*, 6045 – 6049.

[14] D. S. Germack, C. K. Chan, R. J. Kline, D. A. Fischer, D. J. Gundlach, M. F. Toney, L. J. Richter, D. M. DeLongchamp, *Macromolecules* **2010**, *43*, 3828 – 3836.

[15] A. C. Mayer, M. F. Toney, S. R. Scully, J. Rivnay, C. J. Brabec, M. Scharber, M. Koppe, M. Heeney, I. McCulloch, M. D. McGehee, *Adv. Funct. Mater.* **2009**, *19*, 1173 – 1179.

[16] T.-Y. Chu, O.-K. Song, *Appl. Phys. Lett.* **2007**, *90*, 203512.

[17] a) K.-G. Lim, H.-B. Kim, J. Jeong, H. Kim, J. Y. Kim, T.-W. Lee, *Adv. Mater.* **2014**, DOI: 10.1002/adma.201401775; b) T. W. Lee, Y. Chung, O. Kwon, J. J. Park, *Adv. Funct. Mater.* **2007**, *17*, 390 – 396; c) T.-W. Lee, O. Kwon, M.-G. Kim, S. H. Park, J. Chung, S. Y. Kim, Y. Chung, J.-Y. Park, E. Han, D. H. Huh, J.-J. Park, L. Pu, *Appl. Phys. Lett.* **2005**, *87*, 231106; d) T.-H. Han, Y. Lee, M.-R. Choi, S.-H. Woo, S.-H. Bae, B. H. Hong, J.-H. Ahn, T.-W. Lee, *Nat. Photonics* **2012**, *6*, 105 – 110; e) H. Kim, S.-H. Bae, T.-H. Han, K.-G. Lim, J.-H. Ahn, T.-W. Lee, *Nanotechnology* **2014**, *25*, 014012.

[18] H. Tsao, D. M. Cho, I. Park, M. R. Hansen, A. Mavrinskiy, D. Y. Yoon, W. P. R. Graf, H. W. Spiess, K. Müllen, *J. Am. Chem. Soc.* **2011**, *133*, 2605 – 2612.

[19] S. A. Choulis, Y. Kim, J. Nelson, D. D. C. Bradley, M. Giles, M. Shkunov, I. McCulloch, *Appl. Phys. Lett.* **2004**, *85*, 3890 – 3892.
[20] F. Etzold, I. A. Howard, R. Mauer, M. Meister, T.-D. Kim, K.-S. Lee, N. S. Baek, F. Laquai, *J. Am. Chem. Soc.* **2011**, *133*, 9469 – 9479.
[21] F. Etzold, I. A. Howard, N. Forler, D. M. Cho, M. Meister, H. Mangold, J. Shu, M. R. Hansen, K. Müllen, F. Laquai, *J. Am. Chem. Soc.* **2012**, *134*, 10569 – 10583.
[22] I. A. Howard, R. Mauer, M. Meister, F. Laquai, *J. Am. Chem. Soc.* **2010**, *132*, 14866 – 14876.
[23] H. Detert, D. Schollmeyer, E. Sugiono, *Eur. J. Org. Chem.* **2001**, 2927 – 2938.
[24] M. Jørgensen, K. Norrman, S. A. Gevorgyan, T. Tromholt, B. Andreasen, F. C. Krebs, *Adv. Mater.* **2012**, *24*, 580 – 612.
[25] M. Manceau, E. Bundgaard, J. E. Carle, O. Hagemann, M. Helgesen, R. Søndergaard, M. Jørgensen, F. C. Krebs, *J. Mater. Chem.* **2011**, *21*, 4132 – 4141.

Received: August 9, 2014
Revised: October 9, 2014
Published online on November 27, 2014